Investigation on Doppler Imaging and Chromospheric Activity of the Young Dwarf LQ Hya Based on High-resolution Spectroscopy

Xiang Luo[1,2], Shenghong Gu[1,2,3], Yue Xiang[1,3] , A. Collier Cameron[4] , Kang-Min Kim[5], Inwoo Han[5,6], and
Byeong-Cheol Lee[5,6]

[1] Yunnan Observatories, Chinese Academy of Sciences, Kunming 650216, People's Republic of China; luoxiang@ynao.ac.cn, shenghonggu@ynao.ac.cn
[2] University of Chinese Academy of Sciences, Beijing 100049, People's Republic of China
[3] Key Laboratory for the Structure and Evolution of Celestial Objects, Chinese Academy of Sciences, Kunming 650216, People's Republic of China
[4] School of Physics and Astronomy, University of St Andrews, Fife KY16 9SS, UK
[5] Korea Astronomy and Space Science Institute, 776, Daedeokdae-ro, Yuseong-gu, Daejeon 305-348, Republic of Korea
[6] Korea University of Science and Technology, Gajeong-ro, Yuseong-gu, Daejeon 305-333, Republic of Korea
Received 2022 February 10; revised 2022 March 25; accepted 2022 April 20; published 2022 May 23

Abstract

We have obtained four Doppler images of LQ Hya in 2005 November–December, 2006 November–December, 2008 November, and 2014 January–February using high-resolution spectra obtained at three different observing sites. All of the surface maps show that the spots of LQ Hya are in bimodal distribution, i.e., in polar/high-latitude and low-latitude regions. Its chromospheric activity indicators exhibit obvious rotational modulations that are correlated with the simultaneous light curves, except in 2008. The correspondence between the maximum value of chromospheric emission and the low-latitude spot of new reconstructed image is clear, which indicates that both of them are driven by homologous magnetic field. The variation of H_α emission over a long time span suggests that the chromospheric plages may implicate a similar active cycle as photospheric spots.

1. Introduction

LQ Hya (HD 82558, GL 355) is a K2V star with magnetic activity. A large number of photometric studies have shown that its rotational period is about 1.60 days. Strong Ca II emission (Bidelman 1981; Heintz 1981), remarkable Lithium absorption (≈200 mÅ; Fekel et al. 1986), and rapid rotation v sin $i \approx 26$ km s^{-1} (Fekel et al. 1986) indicate that this object is in a relatively young evolutionary state. Fekel et al. (1986) suggested that it is not older than 75 Myr and may have just reached at the zero-age main sequence. They also found that it has far-ultraviolet emission, Ca II H&K emission, and filled-in H_α line, and classified it as a BY Dra-type variable star. The almost constant radial velocity of 7.3 ± 0.6 km s^{-1} (Fekel et al. 1986), 8.6 ± 0.5 km s^{-1} (Donati 1999) and 8.4 ± 0.2 km s^{-1} (Donati et al. 2003) indicates that it is a single star.

Observation and analysis on its magnetic activity have been frequently reported. Frasca et al. (2008), Cao & Gu (2014), and Flores Soriano & Strassmeier (2017) shown an anticorrelation between the chromosphere activity and the light variation of LQ Hya. Lehtinen et al. (2022) also found the anticorrelation between its magnetic field strength and surface brightness. Long-term monitoring of the star shows that its chromosphere activity level decreased during 2006–2012 when its brightness increased (Cao & Gu 2014). These mean that its light variation is resulted from the cool spots on the photosphere. Plages and frequent microflares of LQ Hya have been presented (Strassmeier et al. 1993; Saar & Bookbinder 1998; Alekseev & Kozlova 2002; Frasca et al. 2008; Zhang et al. 2014; Flores Soriano et al. 2015; Flores Soriano & Strassmeier 2017), and a few strong flares have been found in

different wavelengths, e.g., in optical (Montes et al. 1999), UV (Ambruster & Fekel 1990; Montes et al. 1999), and X-ray (Covino et al. 2001) observations. High-resolution spectroscopic observations shown that its $H\alpha$ profile was obviously asymmetric (Strassmeier et al. 1993; Alekseev & Kozlova 2002; Frasca et al. 2008; Flores Soriano & Strassmeier 2017), and most of them shown stronger blue peak than red one.

Based on the light curves, Jetsu (1993) found that active longitudes separated by 90° exist on LQ Hya. Berdyugina et al. (2002) also reported two active longitudes, but with an interval of 180°. However, Lehtinen et al. (2012) did not find a stable active longitude in 24 yr photometric data. The activity cycles of around 6–8 yr were suggested (Jetsu 1993; Strassmeier et al. 1997; Oláh et al. 2000; Berdyugina et al. 2002; Messina & Guinan 2003; Kovári et al. 2004; Olspert et al. 2015), and some studies also shown shorter cycles of 2–4 yr (Oláh et al. 2000; Messina & Guinan 2003; Kovári et al. 2004; Oláh et al. 2009; Lehtinen et al. 2016) and longer cycles of 11–18 yr (Oláh et al. 2000; Berdyugina et al. 2002; Messina & Guinan 2003; Kovári et al. 2004; Oláh et al. 2009; Lehtinen et al. 2012, 2016). On the other hand, by means of the Doppler imaging technique, Strassmeier et al. (1993) found obvious low-latitude and polar spots on the surface of LQ Hya. Rice & Strassmeier (1998) compared its surface temperature maps in 1991, 1993, and 1995, and found a stable belt of spots near the equator and a decreased polar feature. Donati (1999) and Donati et al. (2003) found that low-latitude and polar spots exist in their brightness maps, except at epoch 1991.96 when the spots were only detected at low-latitude region. Kovári et al. (2004) obtained 28 Doppler images in 1996 November–December, which show that the spots were confined to the latitude of around 30°, with occasional high-latitude spots and no polar feature. Cole et al. (2015) shown that spots mainly distributed in two latitude regions—near the equator and close to the pole, respectively, based on seven brightness maps obtained from

Table 1
The Observing Log

Date dd/mm/yyyy	HJD 2,400,000+	Phase	Exp. s	S/N raw	S/N LSD	Inst.	Date dd/mm/yyyy	HJD 2,400,000+	Phase	Exp. s	S/N raw	S/N LSD	Inst.
23/11/2005	53698.3988	0.3762	3300	139	609	CES	23/04/2006	53849.0140	0.4439	1200	73	⋯	BOES
24/11/2005	53699.4018	0.0026	3000	133	713	CES	10/12/2003	52983.7723	0.0515	420	167	⋯	HARPS
17/12/2005	53722.3147	0.3130	3600	81	359	CES	09/01/2005	53379.7131	0.3389	600	264	⋯	HARPS
18/12/2005	53723.3498	0.9595	3600	152	900	CES	12/02/2005	53413.7166	0.5760	600	249	⋯	HARPS
20/12/2005	53725.2868	0.1693	3600	45	195	CES	18/03/2005	53447.6291	0.7563	600	175	⋯	HARPS
21/12/2005	53726.2039	0.7420	3600	39	199	CES	19/03/2005	53448.6681	0.4052	600	236	⋯	HARPS
22/12/2005	53727.2285	0.3820	3600	95	442	CES	08/04/2005	53468.6242	0.8689	600	211	⋯	HARPS
28/11/2006	54068.4028	0.4646	3600	110	559	CES	15/04/2005	53475.5866	0.2174	600	203	⋯	HARPS
29/11/2006	54069.4016	0.0884	3600	140	514	CES	04/06/2005	53891.4786	0.9654	600	222	⋯	HARPS
01/12/2006	54071.3780	0.3228	3600	60	516	CES	17/02/2011	55609.6162	0.0396	600	175	⋯	HARPS
06/12/2006	54076.3328	0.4174	3600	82	404	CES	17/02/2011	55609.6235	0.0441	600	159	⋯	HARPS
06/12/2006	54076.3987	0.4585	3600	91	414	CES	17/02/2011	55609.6314	0.0491	700	159	⋯	HARPS
07/12/2006	54077.3870	0.0757	3600	36	223	CES	17/02/2011	55609.6399	0.0544	700	168	⋯	HARPS
08/12/2006	54078.3468	0.6752	3600	97	370	CES	17/02/2011	55609.7683	0.1346	600	192	⋯	HARPS
09/12/2006	54079.3772	0.3188	3600	120	518	CES	17/02/2011	55609.7757	0.1391	600	192	⋯	HARPS
10/12/2006	54080.3497	0.9261	3600	153	551	CES	17/02/2011	55609.7830	0.1437	600	200	⋯	HARPS
10/12/2006	54080.4176	0.9685	3300	126	433	CES	17/02/2011	55609.7903	0.1483	600	192	⋯	HARPS
11/12/2006	54081.3371	0.5428	3600	127	725	CES	21/01/2014	56678.7252	0.7586	450	122	2174	HARPS
11/12/2006	54081.3790	0.5689	3600	97	405	CES	21/01/2014	56678.7308	0.7621	450	120	1835	HARPS
11/11/2008	54782.3926	0.3916	3600	150	628	CES	22/01/2014	56679.8571	0.4655	420	138	2254	HARPS
13/11/2008	54784.3604	0.6206	2400	105	435	CES	22/01/2014	56679.8623	0.4688	420	140	1796	HARPS
13/11/2008	54784.3957	0.6427	3600	128	477	CES	17/02/2014	56705.6972	0.6041	700	188	2121	HARPS
14/11/2008	54785.3793	0.2569	2400	95	564	CES	17/02/2014	56705.7057	0.6094	700	188	2319	HARPS
14/11/2008	54785.4077	0.2747	2400	117	542	CES	18/02/2014	56706.7400	0.2554	600	206	2180	HARPS
16/11/2008	54787.3857	0.5101	3600	130	473	CES	18/02/2014	56706.7473	0.2600	600	207	2033	HARPS
17/11/2008	54788.3771	0.1293	3600	87	346	CES	19/02/2014	56707.7356	0.8772	600	178	⋯	HARPS
08/12/2005	53713.2564	0.6556	1800	272	1306	BOES	19/02/2014	56707.7429	0.8818	600	175	⋯	HARPS
10/12/2005	53715.3065	0.9360	1800	125	1516	BOES	25/04/2014	56772.5234	0.3409	575	174	⋯	HARPS
11/12/2005	53716.2143	0.5029	1800	175	1078	BOES	25/04/2014	56772.5304	0.3453	575	185	⋯	HARPS
12/12/2005	53717.2980	0.1798	1800	178	1120	BOES	26/04/2014	56773.5816	0.0018	575	165	⋯	HARPS
21/04/2006	53846.9976	0.1845	1200	175	⋯	BOES	26/04/2014	56773.5887	0.0062	575	167	⋯	HARPS
22/04/2006	53847.9957	0.8079	1200	182	⋯	BOES	19/05/2014	56796.5509	0.3474	500	174	⋯	HARPS
22/04/2006	53848.0123	0.8183	1200	170	⋯	BOES	19/05/2014	56796.5570	0.3512	500	173	⋯	HARPS
23/04/2006	53848.9973	0.4335	1200	79	⋯	BOES		⋯					

1998–2002. Flores Soriano & Strassmeier (2017) found one weak low-latitude spot and two strong high-latitude spots, and the three spots moving apart from each other during 2011 December and 2012 April. Cole-Kodikara et al. (2019) found a bimodal structure for spot distribution, which is similar to the result of Cole et al. (2015). Lehtinen et al. (2022) also concluded the existence of bimodal spot distribution along latitude based on the surface temperature maps obtained in four years.

This paper aims to analyze the surface structure of the LQ Hya in 2005, 2006, 2008, and 2014 by employing the Doppler imaging technique and to study its corresponding chromospheric activity. We describe the spectral observations and data processing in Section 2. The Doppler imaging results are presented in Section 3, and the analysis of chromospheric activity is given in Section 4. Finally, we discuss and summarize this work in Section 5.

2. Observations and Data Reduction

As shown in Table 1, high-resolution spectroscopic observations for LQ Hya were carried out for the epochs 2005, 2006, and 2008 using the Coudé echelle spectrograph (CES; Zhao & Li 2001) attached to the 2.16 m telescope at Xinglong station of the National Astronomical Observatories, China. The CES data, with a wavelength range from 5500 to 9000 Å, were recorded on

a 1 k × 1k CCD detector. The spectral resolution power is $R = 37,000$. The exposure time of 3600 s was used for most spectra to obtain sufficient signal-to-noise ratio (S/N). In addition, some high-resolution spectroscopic observations were performed with Bohyunsan Observatory Echelle Spectrograph (BOES; Kim et al. 2002, 2007) mounted on the 1.8 m telescope of Bohyunsan Optical Astronomy Observatory, Korea in 2005 December and 2006 April. The BOES provides a wider wavelength range of 3500–10,500 Å, and it uses a 2 k × 4 k CCD detector to record the data. The resolution power of the configuration we used is about 48,000. Furthermore, we also collected 32 public available spectra which were observed with High Accuracy Radial velocity Planet Searcher (HARPS) of the ESO 3.6 m telescope from 2003 to 2014 and reduced with the dedicated HARPS pipeline—Data Reduction Software. The HARPS spectrograph (Mayor et al. 2003) provides a resolving power of about 115,000 with a spectral coverage of 3780–6910 Å.

The observed spectra from CES and BOES were reduced using a dedicated pipeline developed by ourselves based on the IRAF[7] package, including image trimming, bias subtraction, scattered

---

[7] IRAF is distributed by the National Optical Astronomy Observatory, which is operated by the Association of Universities for Research in Astronomy (AURA) under cooperative agreement with the National Science Foundation.

light subtraction, flat-fielding, cosmic ray removal, 1D spectrum extraction, wavelength calibration with the spectra of ThAr lamp, and continuum fitting. For the extracted spectra of HARPS in archive, we normalized them to the continuum by using the CONTINUUM task within IRAF.

It is well known that the Doppler imaging technique needs the data set with a high S/N. Thus, we applied least-squares deconvolution (LSD; Donati et al. 1997) method to obtain the mean line profile with higher S/N for each observed spectrum of four selected data sets, which were taken within short intervals in 2005, 2006, 2008, and 2014 (the ones with S/N values of LSD are in Table 1). During the calculation, the line list containing the central wavelength and depth of atomic lines was obtained from the Vienna Atomic Line Database (Kupka et al. 1999) with a input model atmosphere of effective temperature $T_{eff} = 5000$ K, gravity log $g = 4.5$, and micro-turbulence $\xi_t = 1.5$ km s^{-1} (Cole-Kodikara et al. 2019). The spectral lines in the windows of telluric lines and the chromospheric activity indicators had been removed from the line list. We also corrected the small shifts in radial velocity, caused by the instability of the instrumental state, by subtracting the relative shift value between the telluric LSD profile of each spectrum and the one of the first spectrum in each data set (Collier Cameron 1999). The S/N of each LSD line profile is listed in Table 1. In order to calculate the rotational phase for each observed spectrum, the ephemeris of Cole-Kodikara et al. (2019) was used:

$$HJD = 2445274.22 + 1.601136E. \tag{1}$$

The results are also listed in Table 1.

3. Doppler Imaging

3.1. Line Inversion

To perform Doppler imaging with LSD line profiles, we employed the reconstruction code DOppler Tomography of Stars (DoTS) of Collier Cameron (1992, 1997), which utilizes maximum entropy algorithm (Skilling & Bryan 1984). Two temperature components are assumed in DoTS, which means that the stellar surface consists of unperturbed photosphere and cool spots, and the fraction of the pixel occupied by spots is denoted by the spot filling factor f_i, varying from 0 (no spot) to 1 (maximum spottedness). The spot temperature was set as 3500 K according to Cole-Kodikara et al. (2019). To obtain the specific intensity profiles of photosphere and spot, the LSD profiles of slowly rotating inactive stars with similar spectral types were used as templates (HR 222 (K2V) and HR 248 (M0III) for data sets 1–3, HD 205536 (G9V) and HD 25004 (K6V) for data set 4), which were spectroscopically observed with the same instrument configurations to LQ Hya by using 3 telescopes mentioned above. The variation of continuum intensity of the intrinsic profiles as function of limb angle was simulated with a linear limb-darkening law. The limb-darkening coefficients at the centroidal wavelength of LSD profiles for the photosphere and spot were obtained by linearly interpolating the limb-darkening coefficients of UBVRI pass-bands (Claret et al. 2012, 2013).

As discussed by Collier Cameron & Unruh (1994), the accurate stellar parameters, e.g., projected equatorial rotational speed $v \sin i$, the strength of mapping line and the inclination of the rotation axis, are required to prevent the production of artefacts for Doppler imaging technique. The stellar parameters used in this work are listed in Table 2. We used the same values

Table 2
Adopted Stellar Parameters

Photospheric temperature	$T_{eff} = 5000$ K
Spot temperature	$T_{spot} = 3500$ K
Gravity	log $g = 4.5$
Inclination	$i = 65°$
Rotational velocity	$v \sin i = 26.3$ km s^{-1} (data sets 1-3)
	$v \sin i = 26.7$ km s^{-1} (data set 4)
Rotational period	$P = 1^d.601136$
Metallicity	log[M/H] = 0
Microturbulence	$\xi_t = 1.5$ km s^{-1}

as Cole-Kodikara et al. (2019) for most stellar parameters of LQ Hya except for the projected equatorial rotational speed $v \sin i$, which could be slightly affected by instrument profile and the template star used above. The strength of the mapping line also changed for different data sets due to the different instrument broadening. The errors in both of these two parameters will introduce similar artifacts as demonstrated by Collier Cameron & Unruh (1994), thus we fine-tuned them by χ^2 minimization method proposed by Barnes et al. (2005). In detail, under the number of iterations fixed, we performed reconstructions with these two parameters changed simulta-neously, and determined the best combination by searching for a well-defined minimum in χ^2 values. For each data set, to prevent over-fitting to the LSD profiles during Doppler imaging calculation, the iteration was stopped before the spotted areas started to increase rapidly, which means the noises were involved in the fitting. Four optimal spot maps were derived finally, which are displayed in Figure 1, and the corresponding profile fitting is plotted in Figure 2.

Surface differential rotation (SDR) and spot evolution maybe introduce artificial features in the reconstructed images, especially for the 2005 and 2014 data sets, which have long time spans of 28 days. Donati et al. (2003) found that the SDR of LQ Hya is not constant—it was close to the case of rigid body rotation in 1996, then changed to k = (Ω_{eq} − Ω_{pole})/Ω_{eq} ≈ 0.053 rad day^{-1} in 2000. Also, as discussed in Section 3.2, the simultaneous light curves of 2014 are not fully consistent with the spectroscopic inversion result, suggesting that SDR (or any type of fast surface variability) may be at work in 2014. Thus, it should be noticed that the details of our Doppler maps are probably affected by the SDR of LQ Hya although the spectral data sampling did not permit to measure it.

3.2. Results

The first panel of Figure 1 shows the reconstructed map with the LSD profiles in 2005. The map exhibits a pronounced polar cap extending to medium latitudes around phase 0.6, and some low-latitude spots appear around 0°–30°. Three stronger low-latitude spots are located near phases 0.15, 0.4 and 0.95.

Reconstructed map for 2006 (the second panel of Figure 1) shows a similar spot distribution to 2005—a polar cap extending to the equator around the phase 0.1, and low-latitude spots around 20°–40° located around phases 0.36, 0.45, and 0.65. Temperature map obtained by Cole-Kodikara et al. (2019) from 2006 December observations also shows the spots near these phases. But the spot around the phase 0.4 in their map is located at higher latitude and more extended in the longitude direction, compared to the feature in our map. This
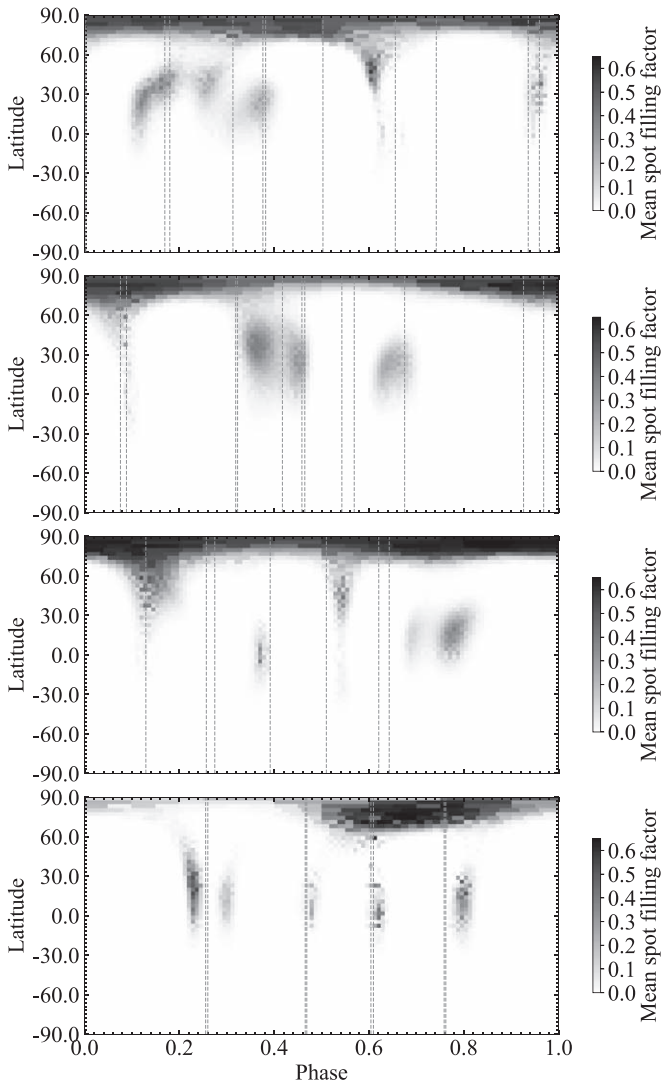
Figure 1. From top to bottom: Mercator projection of Doppler images for 2005, 2006, 2008, and 2014 observational seasons and the phases of observations are marked by vertical dashed lines.

could be due to poor phase coverage which leads to weak constraints on spot latitude as they suggested.

The spot map of 2008 (the third panel of Figure 1) shows a polar cap extending to lower latitudes around phases 0.1 and 0.5 and three low-latitude spots around phases 0.38, 0.68, and 0.78. Although the observations carried out by Cole-Kodikara et al. (2019) is about a month later than ours, the spot structure extending from the pole to low latitude around phase 0.1 is still stable. The low-latitude spots also appear in their map (around the phases 0.3 and 0.7).

The 2014 map (the bottom panel of Figure 1) shows no polar cap, but a high-latitude spot located around phase 0.7, with several weaker low-latitude spots almost uniformly distributed between phases 0.2 and 0.8. Cole-Kodikara et al. (2019) implemented the observations about 2 months earlier than HARPS ones, and their map also shows spot around the phase 0.48, but no other low-latitude spots. The high-latitude spot in their map is located nearly opposite hemisphere to ours. It is quite possible that the fast spot evolution was happened then, which can be inferred from the variation of the corresponding two light curves.

Bimodal distribution–namely, spots that appear in polar/high-latitude and low-latitude regions and are absent in midlatitude region–has been frequently reported. The new reconstructed maps at four epochs also exhibit bimodal distribution, i.e., a polar/high-latitude spot which sometimes extends to lower latitudes, with a few isolated low-latitude spots. The longitude-averaged spot filling factors of our surface maps as functions of latitude have been shown in the left panel of Figure 3. For the 2008 epoch, the bimodal feature is indistinct, which is caused by the features extending from the polar region to midlatitude region rather than individual midlatitude spots.

The latitude-summed spot filling factors as functions of phase (light gray) and the light curves close to our observing time obtained from Lehtinen et al. (2016) are shown in the middle and right panels of Figure 3. In the middle panel of Figure 3, we also show latitude-summed spot filling factors for the latitude regions of 0°–60° (dark) and 60°–90° (gray) as functions of phase. Since we mainly concern with the distribution of spots along phase, rather than the absolute intensity, we use the latitudinal sum instead of the average for easy comparison. For 2005 and 2008 epochs, the locations where the latitude-summed spot filling factors (light gray) are strongest and in good agreement with the phases of minima of light curves. It is difficult to say whether the minimum of the light curve results from the polar (gray) or low-latitude spots (dark), since the phases corresponding to the stronger latitude-summed spot filling factors in these two latitude regions are almost coincident. For the 2006 epoch, the light-curve minimum is clearly associated with low-latitude spots. Photometric data contemporaneous with our 2014 map is absent. The minimum of the light curve of the previous month (blue dots) is located around phase 0.5, while around that phase our reconstructed map shows a very weak feature. Despite the poor sampling, the light curve of the third month (red dots), which is flatter than the one of the first month (blue dots), seems to better correspond to the evenly distributed low-latitude spots of our map. When we compare the first light curve (blue dots) with the reconstructed map of Cole-Kodikara et al. (2019), whose observations were carried out two months earlier than HARPS ones, they are in good agreement. Two Doppler images acquired only two months apart by us and Cole-Kodikara et al. (2019), with marked difference, as well as varying light curves within three months, indicate that the surface structure of LQ Hya may undergo rapid evolution during 2013 December to 2014 February.

4. Chromospheric Activity

4.1. Spatial Connection between Chromosphere and Photosphere

The rotational modulation, which is produced by photospheric and chromospheric active regions lasting for several rotational periods, may be detected by light curves and chromospheric activity indicator time series. Radick et al. (1998) found that the anticorrelation exists between the variation of chromospheric Ca II H & K emission and light curve for young stars, and turns to positive correlation for old stars. This suggests that, as stars evolve at the main sequence, the dominant feature in photosphere changes from spots to faculae. We calculated the flux integrals of the observed activity indicators Ca II H & K, H_β, H_α, Ca II infrared triplet
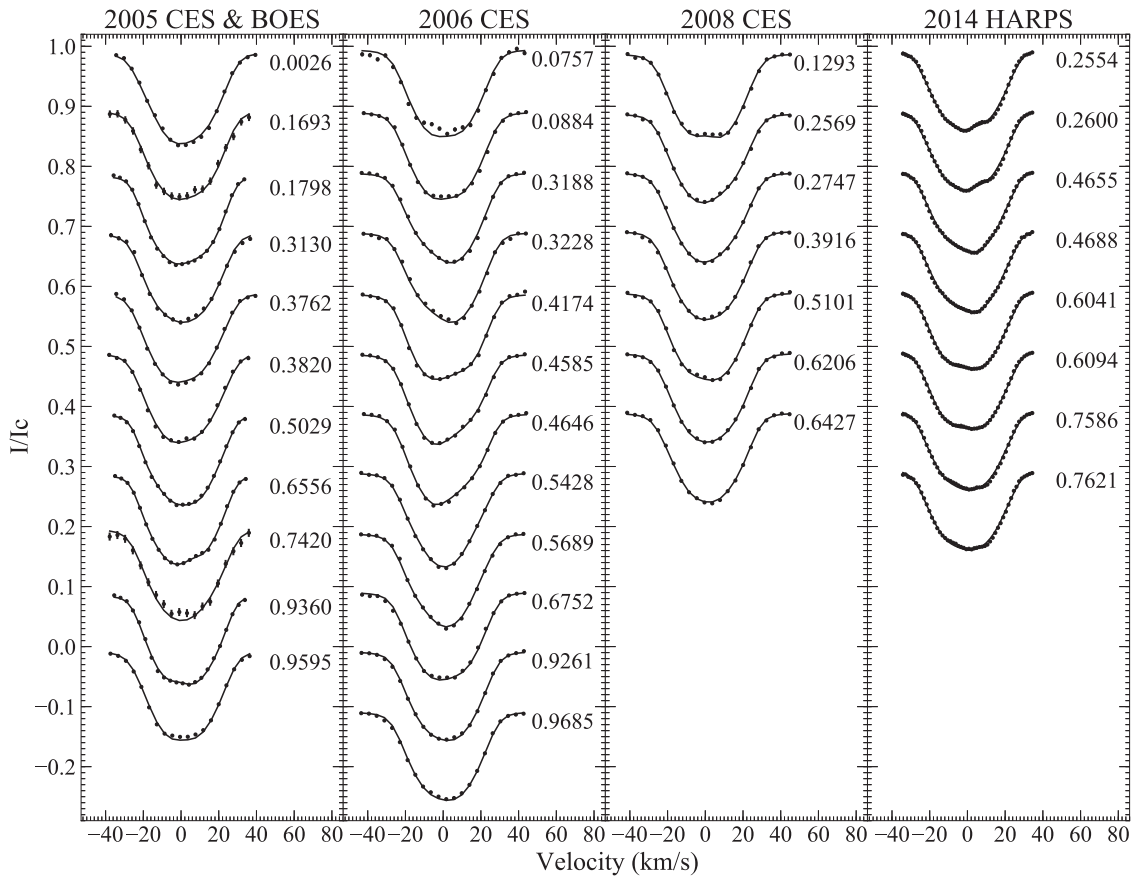
Figure 2. The LSD profiles (points with error bars) and the maximum entropy solutions (solid lines). The value at the right-side of each profile indicates the corresponding observing phase.
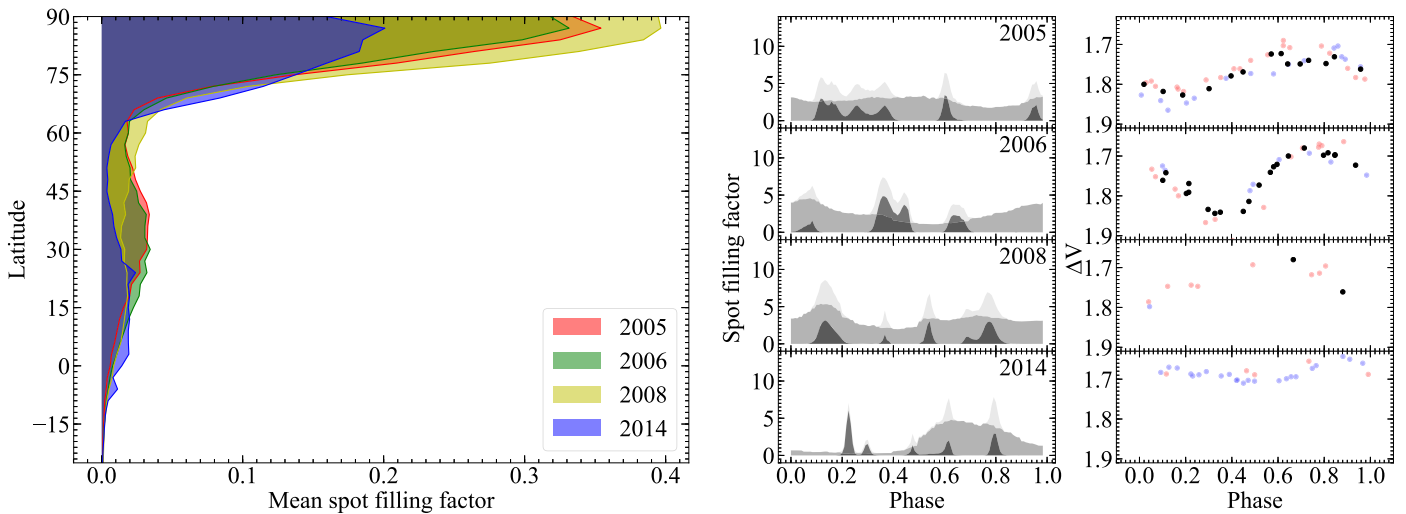

Figure 3. The left panel shows the mean filling factor as a function of latitude for 2005, 2006, 2008, and 2014 observational seasons. The middle panel shows the latitude-summed spot filling factors for the latitude regions of 0° to 60° (dark), 60° to 90° (gray), and 0° to 90° (light gray) as functions of phase. The nearly simultaneous light curves, obtained by Lehtinen et al. (2016), are displayed in the right panel. The black dots represent the light curve in the same observing month as the spectra, and the blue and red dots represent the light curves in the previous and subsequent months, respectively.

(IRT) $\lambda8498$, $\lambda8542$, and $\lambda8662$ lines in 2005 and 2006 data sets, Ca II IRT and H_α lines in the 2008 data set, and Ca II H & K, H_β, H_α lines in the 2014 data set. We show them in Figure 4. Even if the indicators of CES spectra in 2006 and 2008 were already analyzed by Cao & Gu (2014), they were still included in the present analysis so as to construct a

uniform measurement for the further discussion, because the authors used a different method to measure these indicators.

In 2005, although the slight scatter exists in the flux integrals of H_β, H_α, Ca II IRT lines, the synchronized rotational modulation is still clear for all of them. For the observations in November–December, the chromospheric emission shows
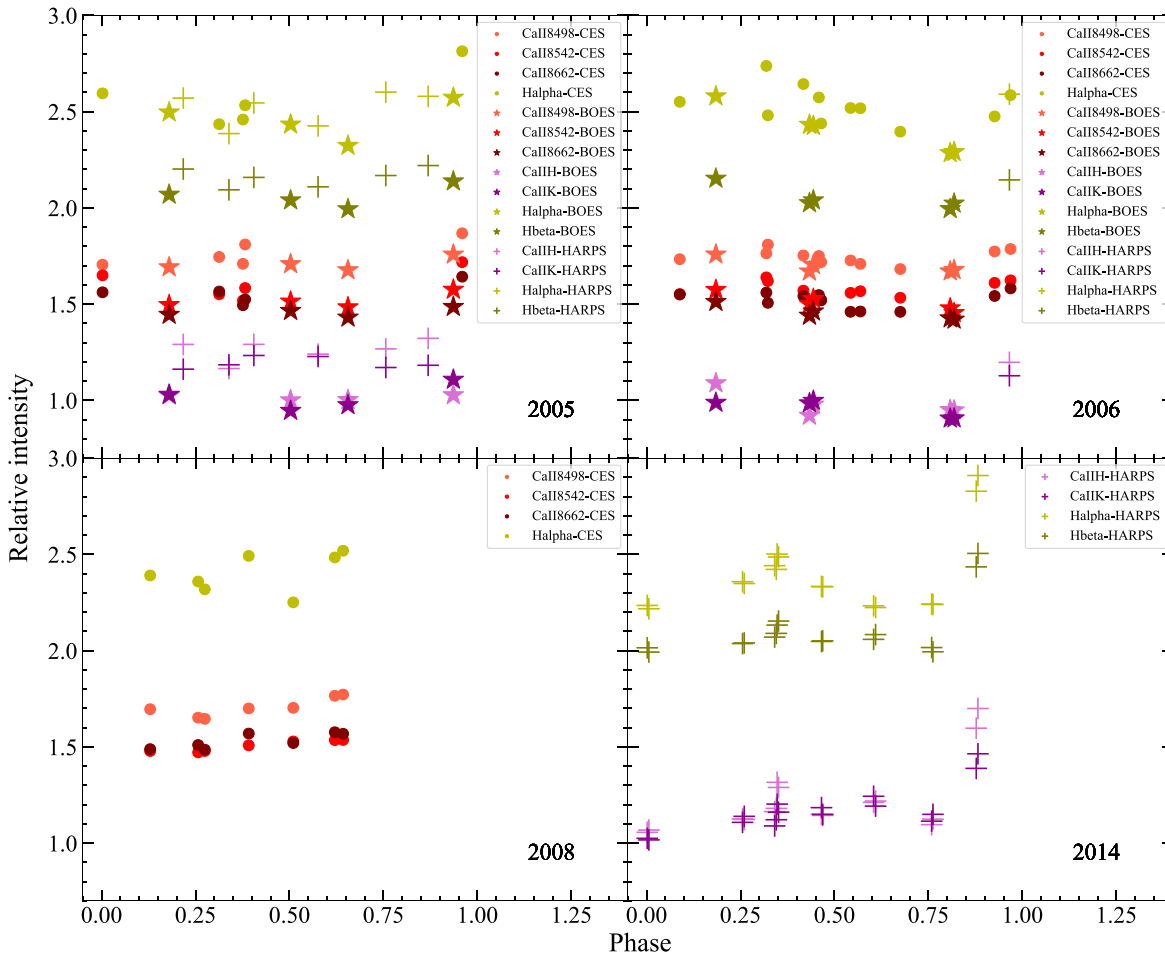
Figure 4. Flux integrals vs. rotational phase for Ca II H&K, H_β, H_α, Ca II IRT lines. Vertical offsets (2.6 for H_α, 1.0 for H_β) are applied for better display.

the primary maximum near the phase 0.95, the secondary one near phase 0.3 and the minimum near the phase 0.8. The results of HARPS (plus) appear to be flatter, which may be due to the fact that the spectra were observed at least 7 months earlier than CES and BOES, which results in the active regions changed. There is an obvious anticorrelation between the chromosphere activity time series and the light curve (see Figure 3). Furthermore, our surface map shows that the spots are concentrated near the phase 0.3 which is corresponding to the secondary maximum of chromosphere emission.

The rotational modulation in 2006 has been reported by Cao & Gu (2014). In addition to the same data as used in Cao & Gu (2014), we added five spectra of BOES and one spectrum of HARPS, all of which show the same modulation, i.e., the strongest activity is near phase 0.4 and the quietest region is near the phase 0.8, and the strongest chromospheric activity may be homologous with the spots near phase 0.4 in the reconstructed map. The anticorrelation exists between the time series of all activity indicators used here and the light curve of 2006.

Unfortunately, the phase coverages both in light curves and spectra are too poor to carry out a reliable analysis in 2008. In 2014, the chromospheric activity modulation which is anticorrelated with the corresponding light curve, is clear except for two points near the phase 0.9 (flare event). The enhanced activity around phase 0.35 may be related to spots located at phases 0.2–0.3 in our reconstructed map.

In the H_α line, the double-peak structure persisted during all of the observing runs, and the examples in 2011 February (green), 2014 January–February (olive), and 2014 April–May (navy blue) were given in the left panel of Figure 5. It is apparent that the blue peak was stronger, or the two peaks were of equal intensity, we did not find any case with stronger red peak.

To explore the long-term spatial connection between the photosphere and the chromosphere, we show the H_α flux integrals (black dots), the light curves (gray dots) and the mean spot filling factors (red dots) in the right panel of Figure 5. In particular, in order to show the relationship between the light curves and H_α flux integrals, we did not invert the y-axis of the light curve following the convention, and the mean spot filling factors were enlarged by a factor of 10 to better display the relative variation. As shown in this Figure, overall chromospheric activity and photospheric activity levels were higher between 2005 and 2006, and decreased gradually after 2007. The mean spot filling factors also follow this trend. A few H_α flux integrals exhibit larger values comparing with the trend mentioned above, which are due to occasional flare events. In addition, the larger mean spot filling factor in 2008 may be attributed to the stronger polar spots. Therefore, there is a clear connection between photospheric and chromospheric activities during 2003–2014.
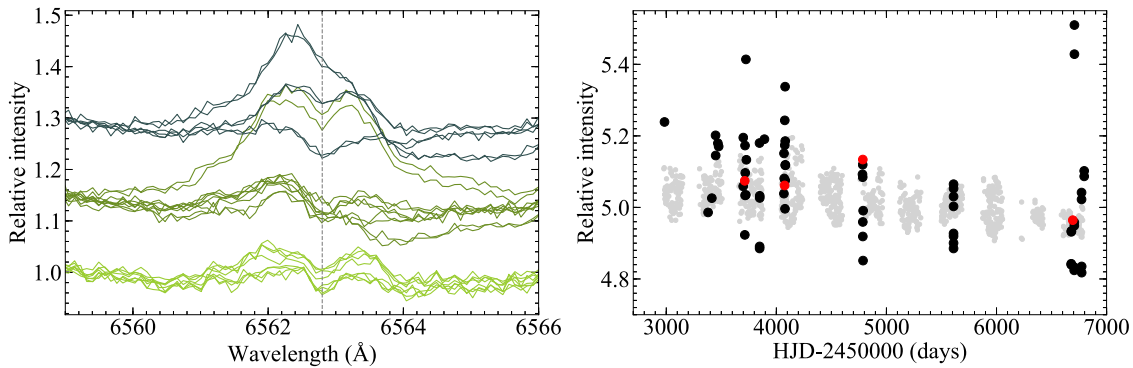
Figure 5. In the left panel, the H_α profiles observed in 2011 February (green), 2014 January–February (olive), and 2014 April–May (navy blue) are plotted from bottom to top. In the right panel, long-term behavior of the H_α flux integrals (black dots), light curves (light gray dots) obtained by Lehtinen et al. (2016) and mean spot filling factors (red dots) are shown from 2003–2014. For better display, we vertically shift the mean spot filling factors which are enlarged by a factor of 10 and the light curves by 4.7 and 3.28, respectively.

4.2. Flare Event

Montes et al. (1999) reported the optical and ultraviolet observations of a strong flare event, and Flores Soriano et al. (2015) also reported possible frequent low-level flare activity on LQ Hya. The HARPS 2014 observations indicate abruptly enhanced activity at the Ca II H & K, H_β, H_α lines of two observed spectra around the phase 0.9 (see Figure 4). In addition, they also exhibit significant stronger emissions in He I $\lambda 3888$, H_ϵ, He I D_3, and Na I D1&D2 lines; Figure 6 is an example. The observed spectrum (dark line) and the mean spectrum (gray dots) of spectra with weak activity around phases 0.75 and 0.45 observed on 2014 January 21 and 22 are shown in the left panel, and the corresponding residual spectrum is shown in the right panel. Moreover, we also found small central reversals in Mg I b triplet $\lambda 5167$, $\lambda 5172$, $\lambda 5183$, and He I lines of 4921.93, 5015.68, and 6678.15 Å. The H_ϵ, H_β, and H_α lines show broad emission wings (about 270 km s^{-1} for H_α), and the He I D_3 line shows distinct emission, even in the original observed spectrum. All of those activity indicators show similar behavior to that found by Montes et al. (1999), suggesting a strong flare event.

To estimate the flare energy release, we used the spectral subtraction technique (Barden 1985; Montes et al. 1995) to obtain pure emission in H_α line by subtracting a synthesized spectrum constructed through artificially rotationally broadened, radial velocity shifted for the spectrum of an inactive star with the similar spectral type (HD 205536, G9V). The observed, synthesized, and subtracted spectra are shown in Figure 7 as an example. Since the two spectra around phase 0.9 show similar activity level, we calculated the flare energy by taking the mean value of 2.147 ± 0.061 Å of the equivalent widths (EWs) of two residual spectra. First, we used the calibration of Hall (1996) to obtain the continuum flux near the H_α line with a color index $B-V = 0.87$ (Koen et al. 2010; Kiraga 2012), and then multiplied by the EW value to obtain the absolute flux $F_{H_\alpha} = 3.4 \times 10^6$ erg cm^{-2} s^{-1}, and luminosity $L_{H_\alpha} = 1.34 \times 10^{29}$ erg s^{-1} that the flare released in H_α line. The estimated energy is of the same order of magnitude as the one of the flare found by Montes et al. (1999), but slightly smaller.

5. Discussion and Conclusions

We have obtained four maximum entropy reconstructed images of LQ Hya for 2005 November–December 2005, 2006

November–December, 2008 Nov, and 2014 January–February. The phase coverage of observations in 2005 and 2006 is relatively complete, and for 2008 and 2014 observations it is about 50% complete. Cole-Kodikara et al. (2019) derived its surface maps for nearly same periods in 2006, 2008, and 2014. The comparison between the two sets of Doppler imaging indicate good correspondence of spots around phases 0.4 and 0.65 in 2006, phases 0.1, 0.38, and 0.68 in 2008, and phase 0.48 in 2014, further suggesting that these spots are real. The reconstructed image for 2005 can be thought to be real due to its data set with good phase coverage.

Our results show that the surface structure of LQ Hya typically exhibits as a polar spot (sometimes extending to low-latitude regions) and several detached low-latitude spots. Such bimodal distribution had been reported in previous studies (Donati 1999; Donati et al. 2003; Cole et al. 2015; Cole-Kodikara et al. 2019; Lehtinen et al. 2022). In young fast-rotating stars, where the Coriolis force rather than buoyancy is the dominant factor, the flux tube tends to be parallel to the axis of rotation and thus usually results in polar caps or high-latitude spots (Schuessler & Solanki 1992; Schuessler et al. 1996). Donati (1999) suggested that the poloidal and toroidal magnetic structures should be generated close to the stellar surface rather than in the overshoot layer at the bottom of the convective envelope like the Sun, so even for rapidly rotating stars with magnetic fluid dominated by the Coriolis force, spots still can appear at low latitudes. Kovári et al. (2004) proposed that the suppression of the Coriolis force by small-scale turbulence and other effects (Choudhuri & D'Silva 1990; D'Silva & Choudhuri 1991) may partly explain the emergence of spots at low latitudes in LQ Hya. On the other hand, numerical simulations of a dynamo dominated by nonaxisymmetric component show high-latitude and weak low-latitude magnetic features for stars with about 20 times of the solar rotational rate (Viviani et al. 2018). Lehtinen et al. (2022) suggested that the strong polar spot and weaker low-latitude spots have different origins. According to their Zeeman Doppler imaging results, polar spots are mainly related to the radial and meridional field, and equatorial spots are mainly related to the azimuthal field.

Chromospheric activity indicators of LQ Hya show significant rotational modulation, except for 2008 observations with a larger dispersion probably due to additional microflare events. The anticorrelation between surface map and chromospheric activity is evident by comparing Figures 3 and 4. The extremely wide emission line wings in
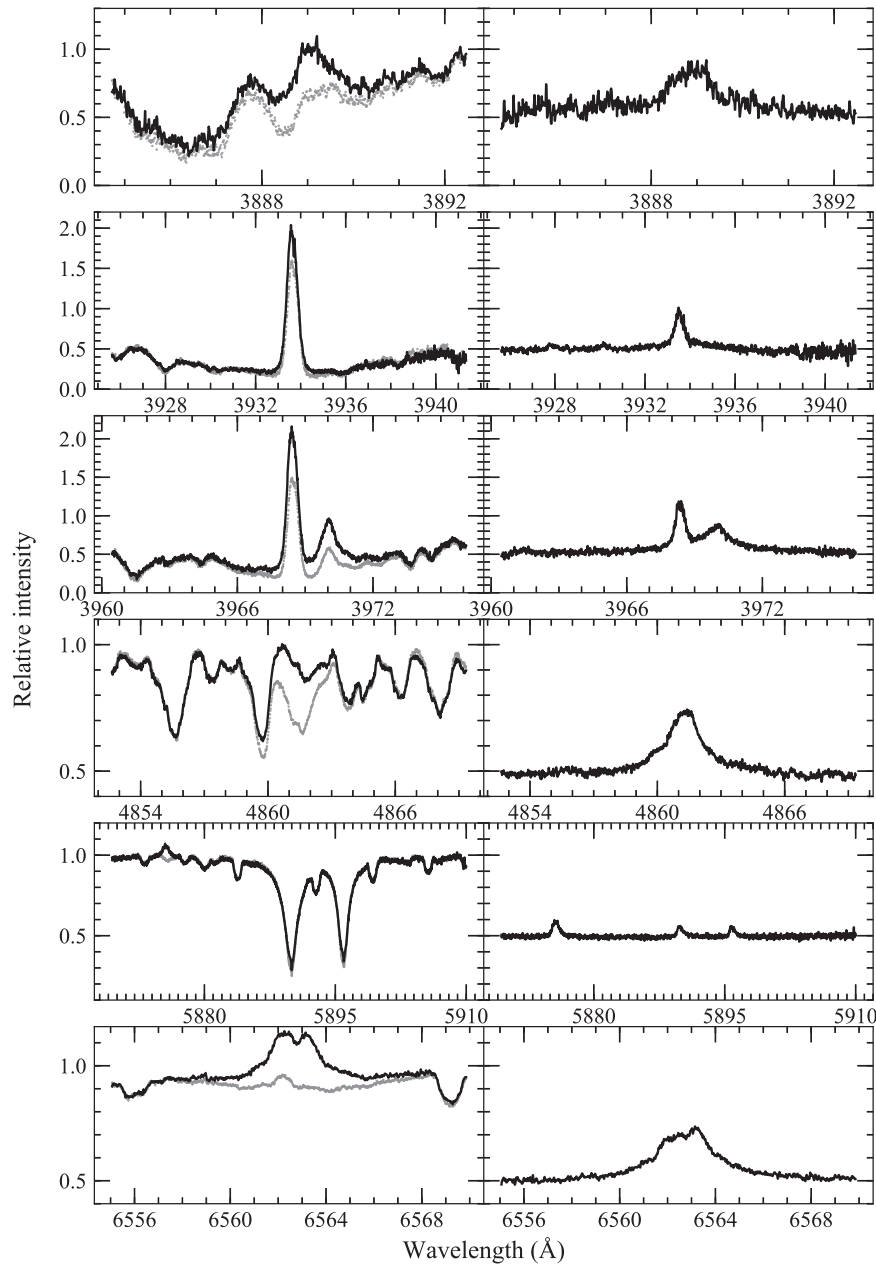
Figure 6. From top to bottom: the observed spectra (solid line) on 2014 February 19 and the mean of quiescent spectra observed on 2014 January 21 and 22, (gray dots) with He I 3888 Å, Ca II H&K, H_ϵ, H_β, He I D_3, Na I DI&D2, and H_α are displayed in the left panel, and the corresponding residual spectra are displayed in the right panel.

H_α, H_β, and H_ϵ lines, and the emission state of He I D_3 line indicate a strong flare event occurred around phase 0.9 in 2014. On the Sun, strong flare eruptions usually root in two magnetic regions with opposite polarities (Toriumi & Wang 2019). Comparing with the Zeeman Doppler imaging results of Lehtinen et al. (2022; their longitude axis is mirrored with respect to our phase axis), two large magnetic regions with opposite polarities around phase 0 in their radial, meridional, and azimuth fields persisted from 2011–2016, maybe associate with the detected strong flare event.

As shown in the left panel of Figure 5, the double-peak structure is stably present in all spectra, although their relative intensities vary with activity level (or rotation). The blue emission peaks are always stronger than red ones, except

during the flare event where the two peaks are of comparable intensity. We do not find any obvious case with stronger red peak. The asymmetric spectral line profile can be attributed to the chromospheric velocity fields and rotational modulation of bright plages in LQ Hya (Strassmeier et al. 1993; Alekseev & Kozlova 2002; Frasca et al. 2008). As seen in the right panel of Figure 5, from 2003–2006, H_α emission is significantly stronger, in 2007 the emission intensity of H_α line changes to be weaker. The change in H_α line emission is almost synchronized with the spot activity, which suggests a probable chromospheric activity cycle similar to spot cycle. Generally, the periodicity of chromospheric activity in such young stars is suspicious (Vaughan & Preston 1980; Vaughan 1980), but we think this probably is because of the disturbing by occasional flare events, like the case at phase 0.9 in 2014.
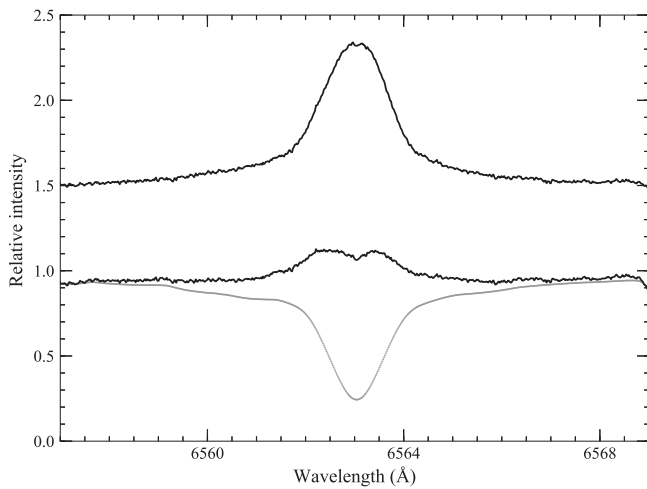
Figure 7. The observed (the lower solid line), synthesized (the dotted line), and subtracted spectrum (upper solid line) for H$_\alpha$ line. The subtracted spectrum is shifted for better display.

ORCID iDs

Yue Xiang https://orcid.org/0000-0001-6580-9378
A. Collier Cameron https://orcid.org/0000-0002-8863-7828
Byeong-Cheol Lee https://orcid.org/0000-0002-2783-0755

References

Alekseev, I. Y., & Kozlova, O. V. 2002, A&A, 396, 203
Ambruster, C., & Fekel, F. 1990, BAAS, 22, 857
Barden, S. C. 1985, ApJ, 295, 162
Barnes, J. R., Collier Cameron, A., Lister, T. A., Pointer, G. R., & Still, M. D. 2005, MNRAS, 356, 1501
Berdyugina, S. V., Pelt, J., & Tuominen, I. 2002, A&A, 394, 505
Bidelman, W. P. 1981, AJ, 86, 553
Cao, D.-t., & Gu, S.-h 2014, AJ, 147, 38
Choudhuri, A. R., & D'Silva, S. 1990, A&A, 239, 326
Claret, A., Hauschildt, P. H., & Witte, S. 2012, A&A, 546, A14
Claret, A., Hauschildt, P. H., & Witte, S. 2013, A&A, 552, A16
Cole, E. M., Hackman, T., Käpylä, M. J., et al. 2015, A&A, 581, A69
Cole-Kodikara, E. M., Käpylä, M. J., Lehtinen, J. J., et al. 2019, A&A, 629, A120
Collier Cameron, A. 1992, in in Surface Inhomogeneities on Late-Type Stars, ed. P. B. Byrne & D. J. Mullan, Vol. 397 (Berlin: Springer), 33
Collier Cameron, A. 1997, MNRAS, 287, 556
Collier Cameron, A. 1999, in ASP Conf. Ser. 185, IAU Colloq. 170: Precise Stellar Radial Velocities, ed. J. B. Hearnshaw & C. D. Scarfe (San Francisco, CA: ASP), 233
Collier Cameron, A., & Unruh, Y. C. 1994, MNRAS, 269, 814
Covino, S., Panzera, M. R., Tagliaferri, G., & Pallavicini, R. 2001, in ASP Conf. Ser., 234, ed. R. Giacconi, S. Serio, & L. Stella (San Francisco, CA: ASP), 101
Donati, J. F. 1999, MNRAS, 302, 457
Donati, J. F., Collier Cameron, A., Semel, M., et al. 2003, MNRAS, 345, 1145
Donati, J. F., Semel, M., Carter, B. D., Rees, D. E., & Collier Cameron, A. 1997, MNRAS, 291, 658
D'Silva, S. Z., & Choudhuri, A. R. 1991, SoPh, 136, 201
Fekel, F. C., Bopp, B. W., Africano, J. L., et al. 1986, AJ, 92, 1150
Flores Soriano, M., & Strassmeier, K. G. 2017, A&A, 597, A101
Flores Soriano, M., Strassmeier, K. G., & Weber, M. 2015, A&A, 575, A57
Frasca, A., Kővári, Z., Strassmeier, K. G., & Biazzo, K. 2008, A&A, 481, 229
Hall, J. C. 1996, PASP, 108, 313
Heintz, W. D. 1981, ApJS, 46, 247
Jetsu, L. 1993, A&A, 276, 345
Kim, K.-M., Han, I., Valyavin, V. G., et al. 2007, PASP, 119, 1052
Kim, K.-M., Jang, B.-H., Han, I., et al. 2002, JKAS, 35, 221
Kiraga, M. 2012, AcA, 62, 67
Koen, C., Kilkenny, D., van Wyk, F., & Marang, F. 2010, MNRAS, 403, 1949
Kővári, Z., Strassmeier, K. G., Granzer, T., et al. 2004, A&A, 417, 1047
Kupka, F., Piskunov, N., Ryabchikova, T. A., Stempels, H. C., & Weiss, W. W. 1999, A&AS, 138, 119
Lehtinen, J., Jetsu, L., Hackman, T., Kajatkari, P., & Henry, G. W. 2012, A&A, 542, A38
Lehtinen, J., Jetsu, L., Hackman, T., Kajatkari, P., & Henry, G. W. 2016, A&A, 588, A38
Lehtinen, J. J., Käpylä, M. J., Hackman, T., et al. 2022, A&A, 660, A141
Mayor, M., Pepe, F., Queloz, D., et al. 2003, Msngr, 114, 20
Messina, S., & Guinan, E. F. 2003, A&A, 409, 1017
Montes, D., Fernandez-Figueroa, M. J., de Castro, E., & Cornide, M. 1995, A&A, 294, 165
Montes, D., Saar, S. H., Collier Cameron, A., & Unruh, Y. C. 1999, MNRAS, 305, 45
Oláh, K., Kolláth, Z., Granzer, T., et al. 2009, A&A, 501, 703
Oláh, K., Kolláth, Z., & Strassmeier, K. G. 2000, A&A, 356, 643
Olspert, N., Käpylä, M. J., Pelt, J., et al. 2015, A&A, 577, A120
Radick, R. R., Lockwood, G. W., Skiff, B. A., & Baliunas, S. L. 1998, ApJS, 118, 239
Rice, J. B., & Strassmeier, K. G. 1998, A&A, 336, 972
Saar, S. H., & Bookbinder, J. A. 1998, in ASP Conf. Ser. 154, Cool Stars, Stellar Systems, and the Sun, ed. R. A. Donahue & J. A. Bookbinder (San Francisco, CA: ASP), 1560
Schuessler, M., Caligari, P., Ferriz-Mas, A., Solanki, S. K., & Stix, M. 1996, A&A, 314, 503
Schuessler, M., & Solanki, S. K. 1992, A&A, 264, L13
Skilling, J., & Bryan, R. K. 1984, MNRAS, 211, 111
Strassmeier, K. G., Bartus, J., Cutispoto, G., & Rodono, M. 1997, A&AS, 125, 11
Strassmeier, K. G., Rice, J. B., Wehlau, W. H., Hill, G. M., & Matthews, J. M. 1993, A&A, 268, 671
Toriumi, S., & Wang, H. 2019, LRSP, 16, 3
Vaughan, A. H. 1980, PASP, 92, 392
Vaughan, A. H., & Preston, G. W. 1980, PASP, 92, 385
Viviani, M., Warnecke, J., Käpylä, M. J., et al. 2018, A&A, 616, A160
Zhang, L., Pi, Q., Zhu, Z., Zhang, X., & Li, Z. 2014, NewA, 32, 1
Zhao, G., & Li, H.-B. 2001, ChJAA, 1, 555